CHAPTER 4

RESULTS AND DISCUSSION

4.1 Differential Scanning Calorimeter (DSC)

Figure 4.1 shows the DSC trace for S1 precursor. In the region below 150°C, there are several endothermic reactions that peaks at 55.4°C which could be assigned to the melting of cobalt (II) nitrate hexahydrate (Robert, 1984). This followed by a second endothermic reaction that peaks at 86.7°C. This could be assigned to the melting of nickel (II) nitrate hexahydrate which melts at 56.7°C and to lithium acetate dihydrate which melts at 70°C. These endothermic peaks could also be contributed by the evaporation of absorbed water and water of crystallization. An exothermic peak is observed at 269.3°C which could be attributed to the formation of a crystalline phase begins to form.

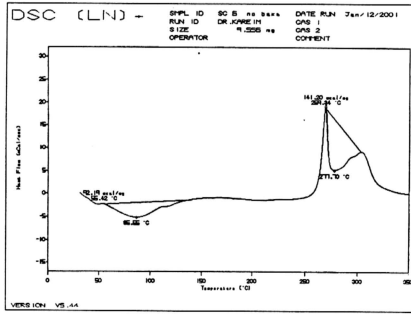

Figure 4.1 DSC trace for S1 precursor

Figure 4.2 shows the DSC trace for S2 precursor. Again two endothermic reaction are observed to take place. One peaking at 50°C and the other peaking at 82.1°C. Again these are attributed to the melting of the nitrate of cobalt and the acetate of lithium and to the removal of absorbed water and water of crystallisation. Then two exothermic peaks are observed; one peaking at 264.1°C and the other at 304.7°C. It is not understood yet whether this is a two phase system or whether the formation of a single crystalline phase begins at the onset temperature of the first exothermic peak and continue to completion at a higher temperature as the shown by the temperature of the second exothermic peak.

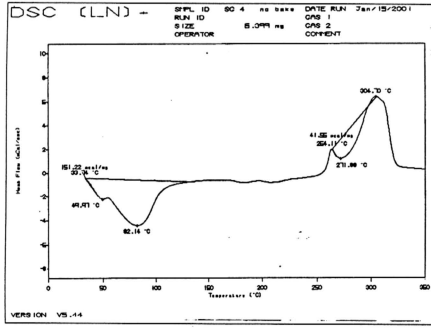

Figure 4.2 DSC trace for S2 precursor

Figure 4.3 shows the DSC trace for S3 precursor. In this trace, it can also be observed that there are several endothermic peaks. The peaks at 41.8°C and 85.2°C can be explained as before but the peak at 120.3°C could be attributed to manganese acetate

which is present in a greater amount compared to sample S2. There is also another endothermic peak at 222.7°C which could not be assigned yet.

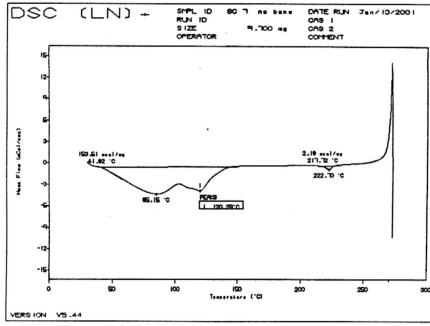

Figure 4.3 DSC trace for S3 precursor

Figure 4.4 shows the DSC trace for S4 precursor. The endothermic reaction can be explained as precursor S3. There are 2 crystallisation peaks and it can be said that the temperature of formation of the crystalline phase is at about 268°C. In short, the temperature of formation of the expected products is as listed in Table 4.1.

Table 4.1 : Formation temperature of products

Sample	Formation Temperature, °C
S1	269.3
S2	264.1
S3	270.9
S4	268.1

The formation temperature for the samples is about the same.

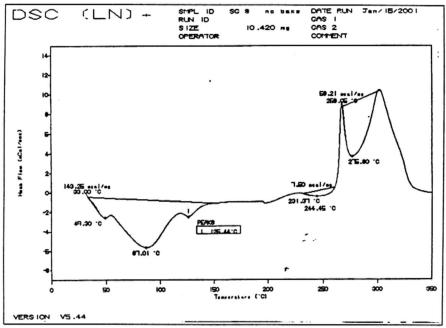

Figure 4.8 DSC trace for S4 precursor

4.2 X-ray diffraction (XRD)

In order to determine the types of materials produced, x-ray diffraction was carried out. Figure 4.5, 4.6, 4.7 and 4.8 list the XRD patterns of the precursors, precursors heated at 400°C, precursors heated at 800°C and precursor heated at 950°C for the same length of time.

From the XRD patterns, some of the precursor materials are totally amorphous while some contain crystalline peaks. The XRD pattern of the precursor designated S1 still shows peaks attributable to LiOAc at about $2\theta = 13^{\circ}$ and 15° and also at $2\theta = 40^{\circ}$ (pattern number: 23-1171). The peaks attributable to nickel nitrate are also observed at $2\theta \approx 21^{\circ}$ and 41° (pattern number: 14-0593). From the XRD pattern of the sample

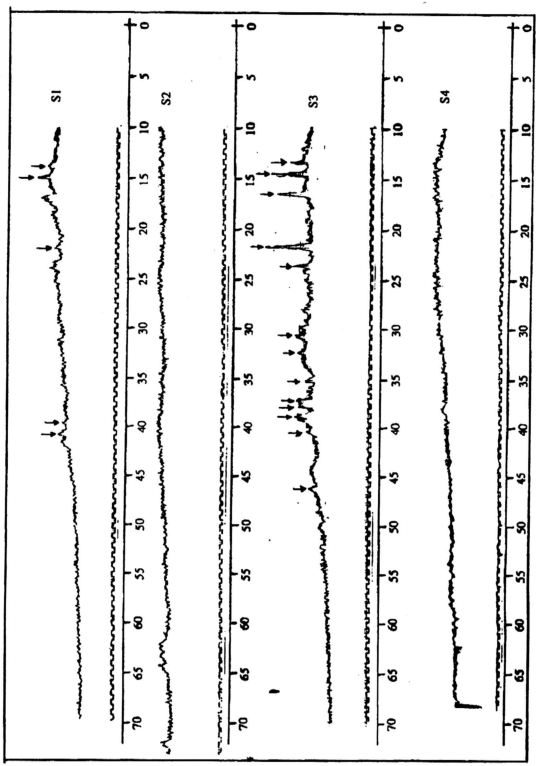

Figure 4.5 : XRD pattern for precursors

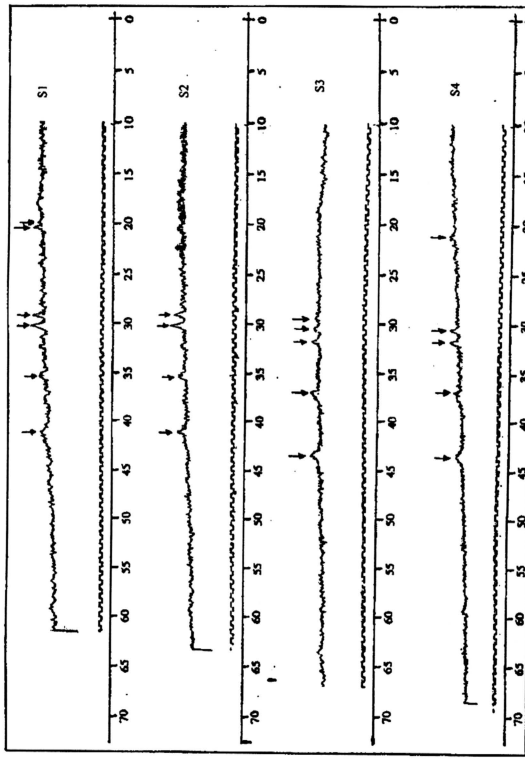

Figure 4.6 : XRD pattern for precursors heated at 400°C

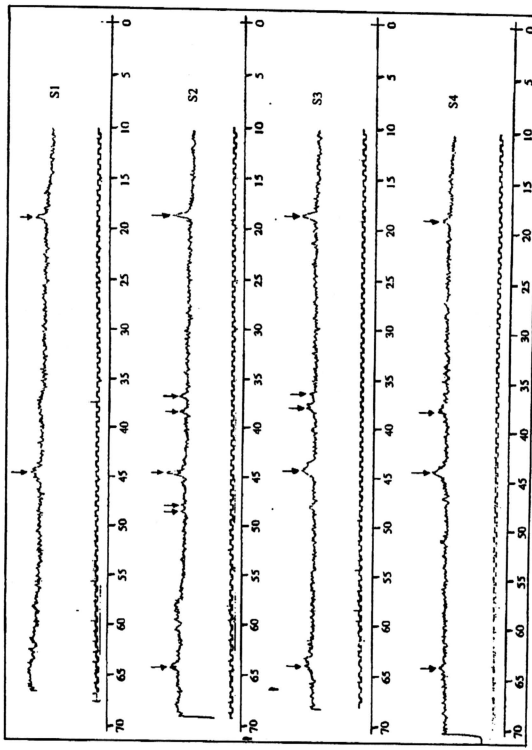

Figure 4.7 : XRD pattern for precursors heated at 800°C

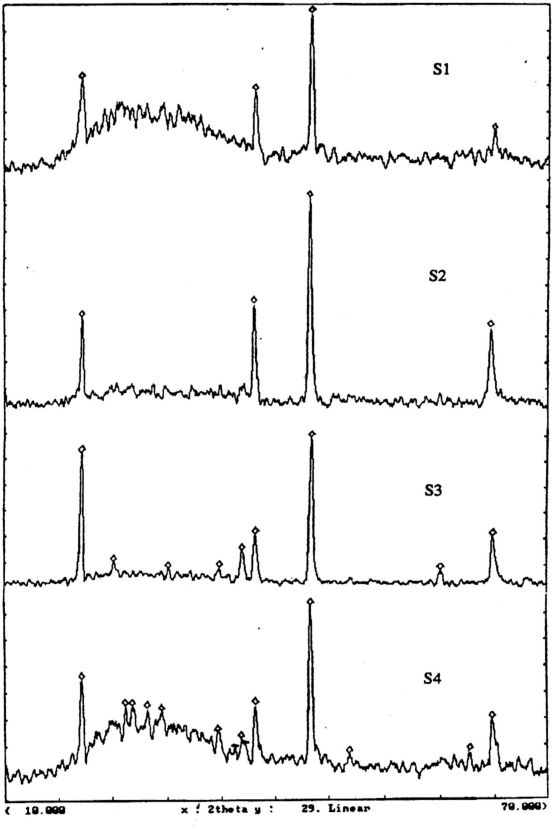

Figure 4:4 : XRD pattern for precursor heated at 950°C

designated S3, there are some peaks that cannot be attributed to any one of the starting chemicals. These are most probably peaks of a new phase, which shows reaction could occur during the 'gel' phase. The peaks that cannot be determined are at $2\theta \approx 32.5^{o}$, 37.2^{o} and 37.8^{o}. The peaks attributable to LiOAc are at $2\theta \approx 14.8^{o}$, 16.5^{o}, 21.7^{o}, 30.7^{o}, 35.2^{o}, 39^{o} and 40.5^{o}, while that of $Ni(NO_3)_2$ (pattern number: 14-0593) are at $2\theta \approx 21.7^{o}$, 30.7^{o}, 35.2^{o} and 46.5^{o} and for $Co(NO_3)_2$ (pattern number: 19-0356) there are 3 peaks at $2\theta \approx 21.7^{o}$, 23.5^{o} and 30.7^{o}. There could be one peak attributable to MnOAc at $2\theta \approx 13.5^{o}$ (pattern number: 14-0724). This peak could also represent a peak of LiOAc. The peaks at 21.7^{o} and 30.7^{o} could be overlap of peaks attributable to LiOAc, $Ni(NO_3)_2$ and $Co(NO_3)_2$, while the peak at 35.2^{o} could be attributable to LiOAc and $Ni(NO_3)_2$.

From the XRD patterns, all the samples heated at 400°C show more defined crystalline peaks. The peaks show the presence of LiOAc, $Ni(NO_3)_2$, $Co(NO_3)_2$ and AlF_3. There are also some peaks that cannot be attributed to the starting materials.

The XRD pattern for the sample designated S1 and heated at 400°C shows peaks attributable to LiOAc at $2\theta \approx 21^{o}$, 29^{o}, 31^{o}, 36^{o} and 41^{o} (pattern number: 23-1171), $Ni(NO_3)_2$ at $2\theta \approx 21^{o}$, 29^{o}, 36^{o} and 41^{o} (pattern number: 14-0593), $Co(NO_3)_2$ (pattern number: 19-0356) at $2\theta \approx 20^{o}$, 29^{o} and 41^{o}. The XRD pattern of the sample heated at 400°C designated S2 shows peaks attributable to LiOAc at $2\theta \approx 29^{o}$, 31^{o}, 36^{o} and 41^{o} (pattern number : 23-1171), $Ni(NO_3)_2$ at $2\theta \approx 29^{o}$, 36^{o} and 41^{o} (pattern number : 14-0593), $Co(NO_3)_2$ (pattern number: 19-0356) at $2\theta \approx 29^{o}$. The XRD pattern of the sample heated at 400°C designated S3 shows peaks attributable to LiOAc at $2\theta \approx 29^{o}$ and 31^{o} (pattern number : 23-1171), $Ni(NO_3)_2$ at $2\theta \approx 29^{o}$ and 43^{o} (pattern number : 14-0593), $Co(NO_3)_2$ (pattern number: 19-0356) at $2\theta \approx 29^{o}$ and the peaks that cannot be determined

are at $2\theta \approx 32^{\circ}$ and 36.5°. The XRD pattern of the sample heated at 400°C designated S4 shows peaks attributable to LiOAc at $2\theta \approx 21^{\circ}$ and 31° (pattern number: 23-1171), $Ni(NO_3)_2$ at $2\theta \approx 21^{\circ}$ and 43° (pattern number: 14-0593), AlF_3 at $2\theta \approx 36.5^{\circ}$ (pattern number: 31-0011) and the peaks that cannot be determined are at $2\theta \approx 32^{\circ}$. As peaks due to the starting materials are still in the diffractogram even though the precursors have been heated at 400°C, the temperatures stated in Table 4.1 must be the temperature at which a crystalline phase begins to form

The XRD patterns for the samples heated at 800°C also show crystalline peaks. However these peaks do not represent peaks due to acetates, nitrates and fluorides. The peaks present in the XRD patterns are shown in Table 4.2. The peaks are compared to

Table 4.2 : 2θ angle for peaks shown for XRD pattern in Figure 4.7

Sample	2θ angle, °
S1	18.5, 45
S2	18.5, 37, 38, 45, 48, 49 and 64
S3	18.5, 36, 37, 44 and 64
S4	18.5, 39, 44 and 64

the findings of Arai et al. (1998). From the comparison, it can be inferred that samples S1, S2, S3 and S4 have a $LiNi_{0.5}Co_{0.5}O_2$ framework. These comparisons were made on the basis that the peak at $2\theta \approx 18.5^{\circ}$ resemble the peak at $2\theta \approx 19^{\circ}$ in the spectrum obtained by Arai et al. (1998). It is known that sample S4 contained aluminium but

unfortunately the peak attributable to aluminium could not be detected from XRD, probably due to its very low content in the sample. Assigning the peak for lithium at 2θ ≈ 18.5° to represent the (003) plane and the peak for Ni at 2θ ≈ 44° or 45° to the (104) plane as in Lee et al (1999), it can be observed that the ratio of the (003)/(104) planes for the S2 precursor heated at 800°C for 5 hours is almost unity. The intensity ratio of (003) and (104) peaks is a key parameter that indicates the degree of the displacement of nickel and lithium ions. Ohzuku et al. (1993) reported that the intensity ratio of (003) and (104) peaks should be more than 1.2 to enhance the electrode performance of $LiNiO_2$. In this work only the product obtained after heating the S2 precursor at 800°C for 5 hours has better crystallinity compound to other samples.

From the XRD patterns in Figure 4.4, all the samples heated at 950°C show crystalline peaks. The XRD pattern for the sample designated S1 and heated at 950°C shows peaks at 2θ ~19°, 38°, 44° and 64°. These peaks are very close to $Li_{0.63}Ni_{1.37}O_2$ as found by Zhecheva and Stoyanova (1993).

The XRD pattern for the sample designated S2 and heated at 950°C also shows peaks at 2θ ~19°, 38°, 44° and 64° as sample designated S1 and heated at 950°C. Both products do not show peaks that due to Co and Mn. Probably both samples need a higher calcination temperature (Zhecheva and Stoyanova, 1993).

The XRD pattern for the sample designated S3 and heated at 950°C shows peaks at 2θ ~19°, 22°, 28°, 34°, 36.5°, 38°, 44°, 58° and 64°. Peaks that was assigned to Ni at 38° is shifted to a lower diffraction angle at 36.5° and the peak at 38° now is assigned to Co. This is also shown by Zhecheva and stoyanova with their sample $Li_{0.83}(Ni_{1.37}Co_{0.1})_{1.17}O_2$. The peak at 2θ ~.58° is also attributable to Co and peak at 2θ ~

22° is also attributable to Ni (Lee et al, 1999). Peaks at 2θ ~ 28° and 34° cannot be attributable to any of the samples reported by Lee et al (1999) or any of the starting materials.

The XRD pattern for the sample designated S4 and heated at 950°C shows peaks at 2θ ~19°, 23°, 24°, 26°, 27° 34°, 36°, 38°, 44°, 58°, 61° and 64°. As compare to the sample designated S3 and heated at 950°C, there are 4 new peaks at 2θ ~ 24°, 26°, 48° and 61° which could be contributed by aluminium.

From the XRD patterns in this work, for samples heated at 950°C, the (003)/(104) ratios are S1 = 0.525, S2 = 0.436, S3 = 0.875 and S4 = 0.489. This shows a loss of lithium due to sublimation when the materials were heated at a temperature above lithium sublimation temperature. It can therefore be inferred that in order to obtain a product with a good crystalline phase, either the heating or calcination time should be lengthened or the calcination temperature be increased but below the sublimation temperature of lithium (850°C). If the calcination temperature is above the lithium sublimation temperature, the material will not be "electrochemically sound".

4.3 IR spectroscopy

The IR spectrum for lithium acetate, nickel nitrate, cobalt nitrate, manganese acetate and aluminium fluoride which are used as starting constituents in some of the samples are as shown in Figure 4.9. The IR spectrum for the precursors for S1, S2, S3 and S4 are as shown in Figure 4.10. The IR spectrum of the precursor heated at 400°C and 800°C respectively are as shown in the Figure 4.11 and 4.12 respectively. All samples including the chemical constituents are spectroscopically wet. From precursor

S1, there are two peaks around ~1670 cm^{-1} and ~1400 cm^{-1}. The band on the lower wavenumber side extends from ~1300 cm^{-1} to ~1550cm^{-1}. The peaks of the FTIR spectrum in these regions for lithium acetate are at ~1419.29 cm^{-1} and ~1559.03 cm^{-1} whereas nickel nitrate are at ~1384.12 cm^{-1} and 1623.11 cm^{-1}. For cobalt nitrate, the peak is at about 1380 cm^{-1}. The band on the higher wavenumber side is extends from ~1600 cm^{-1} to ~1800 cm^{-1}. In this region, only nickel nitrate shows peaks at ~1764.08 cm^{-1} and ~1623.11 cm^{-1}. For sample S2, the band at the higher wave number side, has split into two smaller wavenumbers, one peaking at ~1590 cm^{-1} and the other at ~1680 cm^{-1}. The same is observed for precursors S3 and S4. For precursor S4, these bands are shifted slightly to lower wavenumbers probably due to the interaction with aluminium fluoride.

The FTIR spectrum for the precursors S1 to S4 heated at 400°C for 5 hours confirmed that some reaction has occurred but the main product that is needed has not fully formed. This again strengthens the inference that the temperatures at the onset of the exothermic peaks of the DSC traces and listed in Table 4.1 are the temperatures at which the crystalline phase (probably leading to the required product) begins to form. This can be attributed to the peak at 864 cm^{-1} to 865 cm^{-1} wavenumber which can be assigned to the vibration of λ–OCO. The peak at 1087 cm^{-1} to 1088 cm^{-1} can be assigned to the vibration of ν–CO + C=O which must come from the acetate of lithium as for the precursor S1 and also due to the acetate of lithium for precursor S2 to S4. The incomplete formation of the required product can also be inferred from the peak at 1439.51 cm^{-1} in the band that extend from 1144 cm^{-1} to 1800 cm^{-1}. This peak (1439.51 cm^{-1}) could arise from vibration related to acetate ligands. This therefore suggests the

possible existence of nickel hydroxyl acetate on heating of the precursor. Nickel hydroxyl acetate (Ni(OH)(OAc)) is insoluble in water.

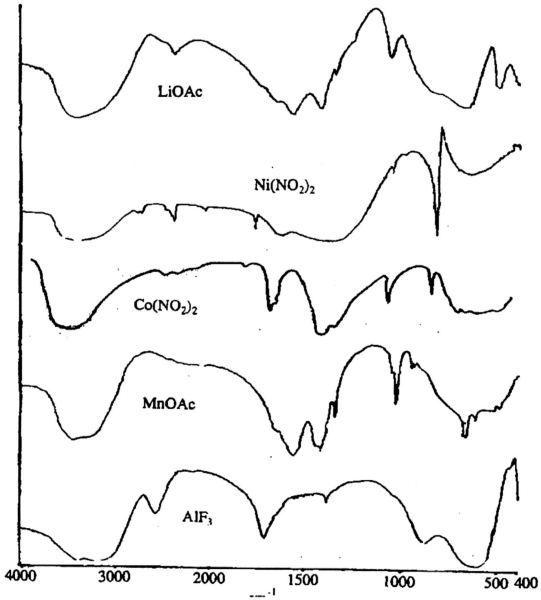

Figure 4.9 : Starting constituents in some of the samples

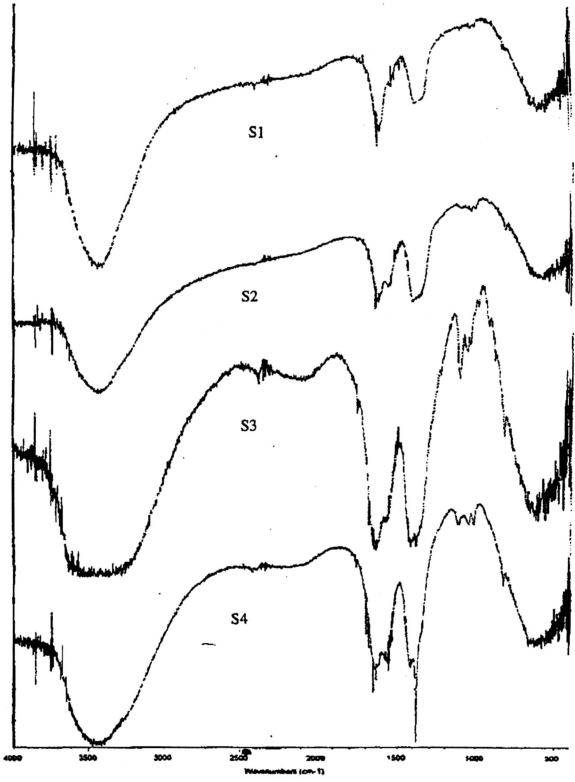

Figure 4.10 : The IR spectrum for the precursors of S1, S2, S3 and S4

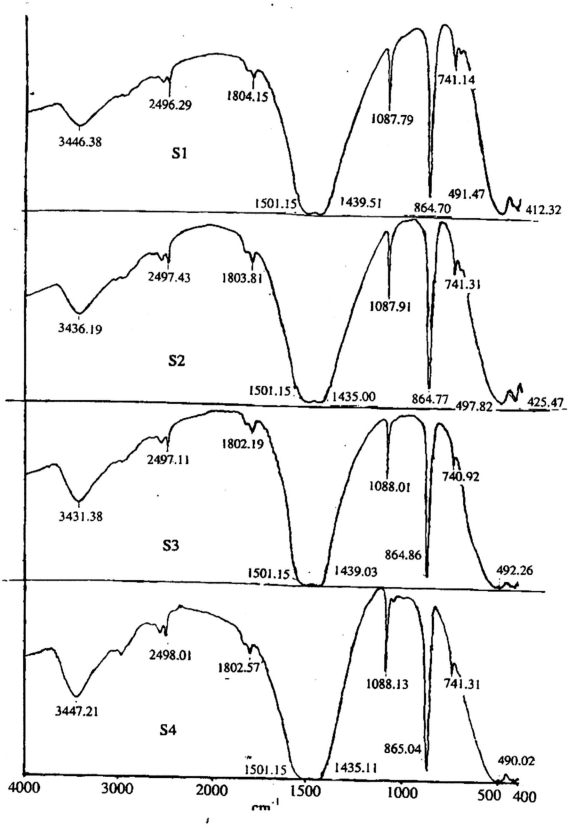

Figure 4.11 : The IR spectrum for the precursors of S1, S2, S3 and S4 heated at 400°C

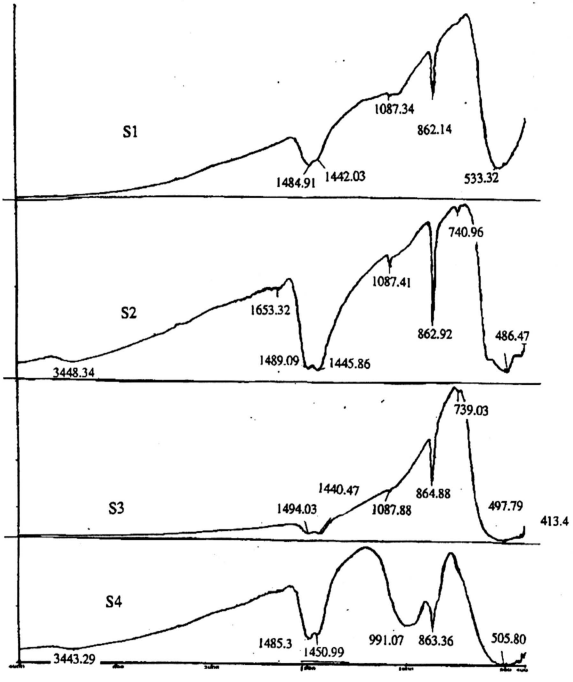

Figure 4.12 : The IR spectrum for the precursors of S1, S2, S3 and S4 heated at 800°C

Since the solvent used to dissolve all the chemical constituents in this work is water, and Ni(OH)(OAc) is insoluble in water, the spectrum of the solid obtained after drying the liquid portion must show a band due to Ni(OH)(OAc). Since nickel nitrate and lithium acetate were used as starting constituents, Ni(OH)(OAc) could have been formed via the reaction below

$$4CH_3COOLi.2H_2O + 2Ni(NO_3)_2.6H_2O + 5O_2 \rightarrow Li_2CO_3 + NiO + CH_3COONiOH + 4NO_2 + 5CO_2 + 2LiOH + 23H_2O$$

or

$$2CH_3COOLi.2H_2O + 2Ni(NO_3)_2.6H_2O + O_2 \rightarrow NiO + CH_3COONiOH + 4NO_2 + 2CO_2 + 2LiOH + 16H_2O$$

The presence of LiOH may be evidenced from the shoulder at ~841cm^{-1} which happens to be present in all samples heated at 400°C. Hence the presence of LiOH in the above equations is justified. The presence of NiO is evidenced by the peak at 741cm^{-1}.

In order to explain the presence of the bands at 864 cm^{-1} and 1088 cm^{-1} which are attributed to carbonates, it is expected that the first reaction mentioned above occurred. The following reactions could also produce carbonates :-

Reaction 1 : $2LiOAc + 2O_2 \rightarrow Li_2CO_3 + 3H_2O + CO_2$

Reaction 2 : $Mn(OAc)_2 + 2O_2 \rightarrow MnCO_3 + 3H_2O + CO_2$

However, reaction 2 is only possible when precursors S2 to S4 are heated at 400°C. It can be observed that the spectrum for precursor S1 to S3 heated at 800°C does not differ much from the spectrum of the same precursors heated at 400°C with the exception with the intensity of Ni(OH)(OAc) band and the carbonate band have reduced in intensity. However there is a difference in the spectrum for S4 precursor heated at 400°C and 800°C. This is due to the existence of a broad band peaking at 991cm^{-1} which could have overlap with the 1088 cm^{-1} band. It is uncertain what this represents, but since this sample contains aluminium floride, it is thus inferred that the change in the band is due to the interaction between aluminium floride with the other chemical constituents or with the by-product of the reaction between these chemical constituents.

Figure 4.13 shows the IR spectrum of the precursor heated at 950°C. Although there is a loss in lithium content as observed in the XRD patterns, peaks attributable to the hydroxyacetates are still observed but the amount is very much reduced. This shows that it is not possible to produce such compounds at low temperature as reported by Prabaharan et al (1997).

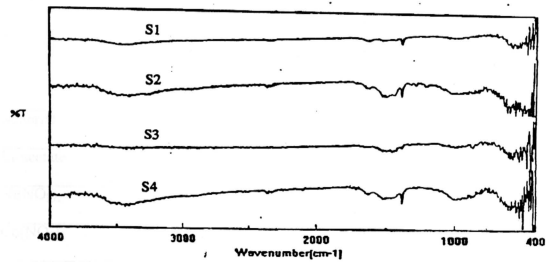

Figure 4.13 : The IR spectrum for the precursors of S1, S2, S3 and S4 heated at 950°C

4.4 EDAX Analysis

The starting materials used for the precursor S1 are as listed in Table 4.3

Table 4.3 : Calculation for amount of chemical used for S1

Material	Weight/g	Molecular weight/g/mole	Mole of material	Number of atoms
Li(acetate)	24.48	102.02	0.24	1.44×10^{23}
$Ni(NO_3)_2$	12.21	290.81	0.042	2.53×10^{22}
$Co(NO_3)_2$	5.238	291.03	0.018	1.08×10^{22}

The starting materials used for the precursor S2 are as listed in Table 4.4

Table 4.4 : Calculation for amount of chemical used for S2

Material	Weight/g	Molecular weight/g/mole	Mole of material	Number of atoms
Li(acetate)	8.16	102.02	0.08	4.82×10^{22}
$Ni(NO_3)_2$	4.07	290.81	0.014	8.43×10^{21}
$Co(NO_3)_2$	1.164	291.03	0.004	2.41×10^{21}
Mn(acetate)	0.49	245.09	0.002	1.20×10^{21}

The starting materials used for the precursor S3 are as listed in Table 4.5

Table 4.5 : Calculation for amount of chemical used for S3

Material	Weight/g	Molecular weight/g/mole	Mole of material	Number of atoms
Li(acetate)	16.32	102.02	0.16	9.64×10^{22}
$Ni(NO_3)_2$	8.14	290.81	0.028	1.68×10^{22}
$Co(NO_3)_2$	1.164	291.03	0.004	2.41×10^{21}
Mn(acetate)	1.96	245.09	0.008	4.82×10^{21}

The starting materials used for the precursor S4 are as listed in Table 4.6

Table 4.6 : Calculation for amount of chemical used for S4

Material	Weight/g	Molecular weight/g/mole	Mole of material	Number of atoms
Li(acetate)	16.32	102.02	0.16	9.64×10^{22}
$Ni(NO_3)_2$	8.14	290.81	0.028	1.68×10^{22}
$Co(NO_3)_2$	1.164	291.03	0.004	2.41×10^{21}
Mn(acetate)	0.98	245.09	0.004	2.41×10^{21}
AlF_3	0.552	138	0.004	2.41×10^{21}

From the calculation of starting materials. The products for precursors heated at 950°C expected as shown in Table 4.7.

Table 4.7 : Expected products

Samples	Products
S1	$LiNi_{0.7}Co_{0.3}O_2$
S2	$LiNi_{0.7}Co_{0.1}Mn_{0.2}O_2$
S3	$LiNi_{0.7}Co_{0.2}Mn_{0.1}O_2$
S4	$LiNi_{0.7}Co_{0.1}Mn_{0.1}Al_{0.1}O_2$

Figure 4.14 to 4.17 shows the EDAX patterns of precursors heated at 950°C. The EDAX pattern for the sample designated S1 and heated at 950°C shows the atomic percentage of Co and Ni at 16.56% and 37.09% respectively. From this atomic percentage data the Ni to Co ratio is 7.418 : 52 or approximately 0.7 : 0.3 taken to the first significant figure only. Hence the chemical formula calculated as $Li_xNi_{0.7}Co_{0.30}O_y$. Since the starting

nickel has an oxidation state of 2+, upon oxidation will become 3+. The same is for cobalt. Thus the charge will +2.1 for Ni and +0.9 for Co. Since the oxidation state for lithium is +1, then for conservation of charge oxygen must have a net charge of -4, implying that there be 2 oxygen atoms in the molecule. Hence the chemical formula for precursor S1 heated at 950°C is $LiNi_{0.7}Co_{0.3}O_2$. By the same method the precursor S2 and S3, both heated at 950°C have the formula $LiNi_{0.7}Co_{0.1}Mn_{0.2}O_2$ and $LiNi_{0.7}Co_{0.2}Mn_{0.1}O_2$ respectively. The precursor S4 heated at 950°C has the formula $LiNi_{0.7}Co_{0.1}Mn_{0.1}Al_{0.1}O_2$. In short, the products have a $LiNiO_2$ structure modified by the presence of Co, Mn and Al.

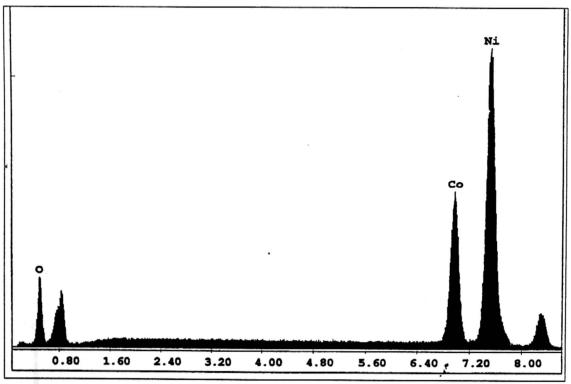

Figure 4.14 : EDAX pattern for precursor S1 heated at 950°C

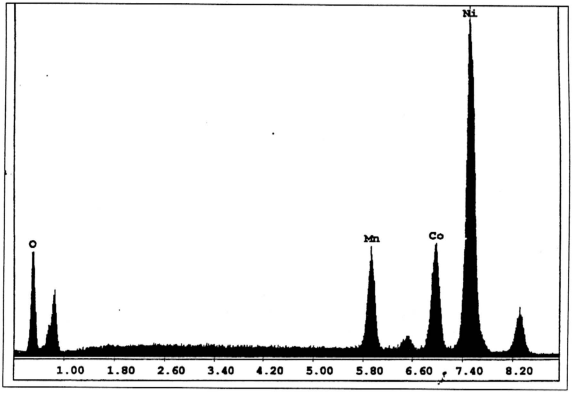

Figure 4.15 : EDAX pattern for precursor S2 heated at 950°C

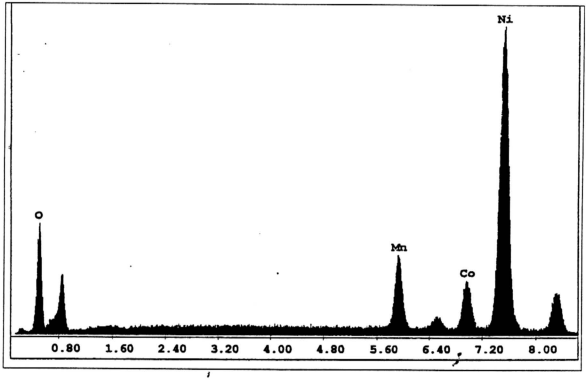

Figure 4.16 : EDAX pattern for precursor S3 heated at 950°C

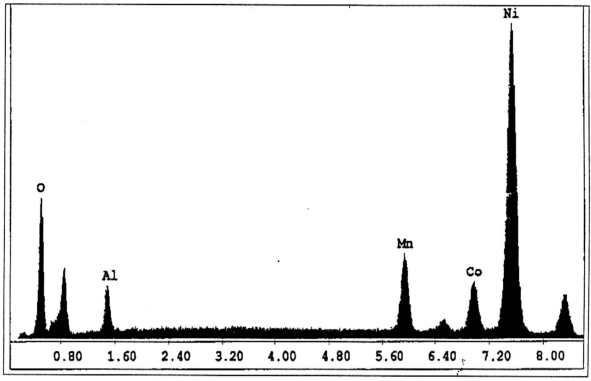

Figure 4.17 : EDAX pattern for precursor S4 heated at 950°C

4.5 Cyclic Voltammetry

From the $LiNiO_2$ structure shown in Figure 2.49 in page 60, the structure of S1, S2, S3 and S4 heated at 400 °C and 800 °C are expected not to deviate much as the cobalt, manganese and aluminium are minor constituents compared to nickel in all 4 materials. Cobalt, manganese and aluminium can occupy any of the original nickel sites in the $LiNiO_2$ structure shown in page 60. Cyclic voltammetry has been done on all four compounds S1, S2, S3 and S4 heated at 400 °C and 800 °C.

The list of possible reduction and oxidation reactions of $Li^+ + e^- \Leftrightarrow Li$ in different environment of nickel, cobalt and manganese are given in Table 4.8. Li^+ is expected to be released (de-intercalate) from $LiNi_{0.7}Co_xMn_yAl_{0.3-(x+y)}O_2$ as the current and voltage is increased during the forward scan and is reduced when Li^+ enters the mixed metal oxide

structure (intercalate). This $Li^+ + e^- \Leftrightarrow Li$ redox couple is expected due to the presence of a loop instead of a staircase wave in the voltammogram. The redox couple of $Fe^{3+}(eq) + e^- \Leftrightarrow Fe^{2+}(eq)$ also gives a loop in aqueous solutions. Therefore all loops in all cyclic voltammograms can be attributed to the redox couple of $Li^+ + e^- \Leftrightarrow Li$ between the same or different transition metals. Since the cobalt, nickel and manganese are first row transition elements, therefore the redox loops can overlap each other making them less defined from each other.

Table 4.8 : Possible reductions and oxidations of $Li^+ + e^- \Leftrightarrow Li$ in different environment of nickel, cobalt and manganese.

Chemical reaction
$Mn^{II}\text{-}Mn^{II} + Li^+ \Leftrightarrow Mn^{III}\text{-}Li\text{-}Mn^{II}$
$e^+ + Mn^{III}\text{-}Li\text{-}Mn^{II} \Leftrightarrow Mn^{II}\text{-}Li\text{-}Mn^{II}$
$Co^{II}\text{-}Co^{II} + Li^+ \Leftrightarrow Co^{III}\text{-}Li\text{-}Co^{II}$
$e^+ + Co^{III}\text{-}Li\text{-}Co^{II} \Leftrightarrow Co^{II}\text{-}Li\text{-}Co^{II}$
$Ni^{II}\text{-}Ni^{II} + Li^+ \Leftrightarrow Ni^{III}\text{-}Li\text{-}Ni^{II}$
$e^+ + Ni^{III}\text{-}Li\text{-}Ni^{II} \Leftrightarrow Ni^{II}\text{-}Li\text{-}Ni^{II}$
$Mn^{II}\text{-}Ni^{II} + Li^+ \Leftrightarrow Mn^{II}\text{-}Li\text{-}Ni^{III}$
$e^+ + Mn^{II}\text{-}Li\text{-}Ni^{III} \Leftrightarrow Mn^{II}\text{-}Li\text{-}Ni^{II}$
$Co^{II}\text{-}Ni^{II} + Li^+ \Leftrightarrow Co^{II}\text{-}Li\text{-}Ni^{III}$
$e^+ + Co^{II}\text{-}Li\text{-}Ni^{III} \Leftrightarrow Co^{II}\text{-}Li\text{-}Ni^{II}$
$Co^{II}\text{-}Mn^{II} + Li^+ \Leftrightarrow Co^{II}\text{-}Li\text{-}Mn^{III}$
$e^+ + Co^{II}\text{-}Li\text{-}Mn^{III} \Leftrightarrow Co^{II}\text{-}Li\text{-}Mn^{II}$

S1- $LiNi_{0.7}Co_{0.3}O_2$

Figure 4.18 and 4.19 show the voltammogram of S1 heated at 400°C and 800°C. For both samples heated at 400°C and 800°C, cyclic voltammetry at $100mVs^{-1}$ show at least 3 redox waves that overlap each other occurring at different potentials.

S2 - $LiNi_{0.7}Co_{0.1}Mn_{0.2}O_2$

Figure 4.20 and 4.21 show the voltammogram of S2 heated at 400°C and 800°C. For both samples heated at 400°C and 800°C, cyclic voltammetry at $100mVs^{-1}$ show at least 5 redox waves (of different currents and redox potentials) that overlap and can be clearly seen.

S3 - $LiNi_{0.7}Co_{0.2}Mn_{0.1}O_2$

Figure 4.22 and 4.23 show the voltammogram of S3 heated at 400°C and 800°C. Cyclic voltammetry at $100mVs^{-1}$ for both 400°C and 800°C gave different number of redox loops, but overlap of the loops still can be seen. For S3 heated at 400°C, cyclic voltammetry at $100mVs^{-1}$ shows 6 redox loops each with different currents. However, for S3 heated at 800°C, cyclic voltammetry at $100mVs^{-1}$ shows only 3 redox loops.

S4 - $LiNi_{0.7}Co_{0.1}Mn_{0.1}Al_{0.1}O_2$

Figure 4.24 and 4.25 show the voltammogram of S4 heated at 400°C and 800°C. Since aluminium is not part of the transition series and do not have 'd' orbitals, it does not take part in the redox reactions of $Li^+ + e^- \Leftrightarrow Li$. Cyclic voltammetry of S4 heated at 800°C, show 4 redox loops, with different currents. A list of Li intercalation can be

thought as Ni^{II}-Li^{+}-Ni^{II}, Co^{II}-Li^{+}-Ni^{II}, Mn^{II}-Li^{+}-Ni^{II} and Co^{II}-Li^{+}-Mn^{II}, with the smallest current is attributed to Co^{II}-Li^{+}-Mn^{II} as the probability of having Co-Mn next together is smallest. As for S4 heated at 400°C, the cyclic voltammetry at $100mVs^{-1}$ showed only one redox loop but the rest are not clearly defined.

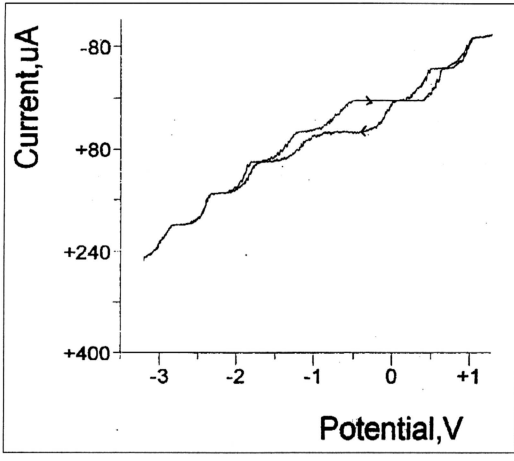

Figure 4.18 : Voltammogram of S1 heated at 400°C.

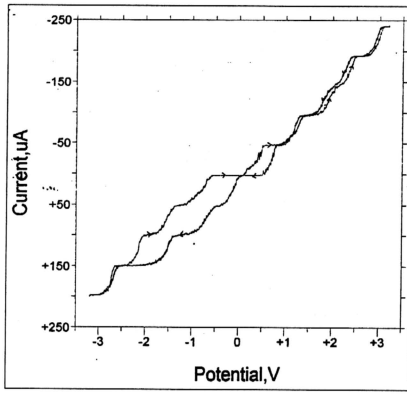

Figure 4.19 : Voltammogram of S1 heated at 800°C.

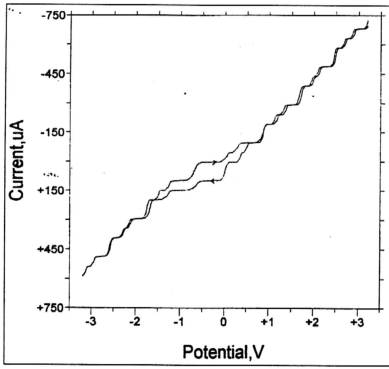

Figure 4.20 :, Voltammogram of S2 heated at 400°C.

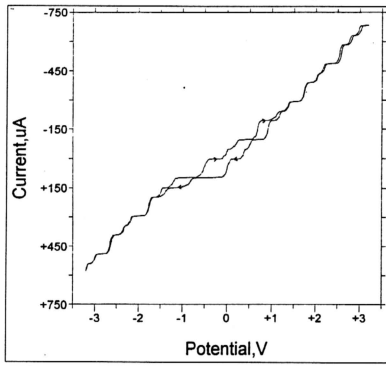

Figure 4.21 : Voltammogram of S2 heated at 800°C.

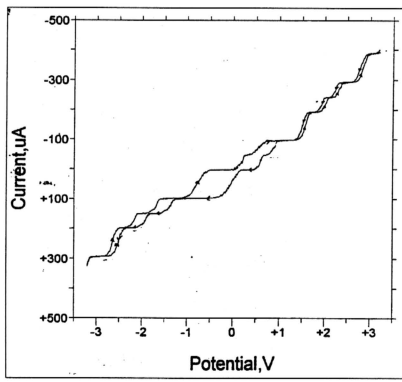

Figure 4.22 : Voltammogram of S3 heated at 400°C.

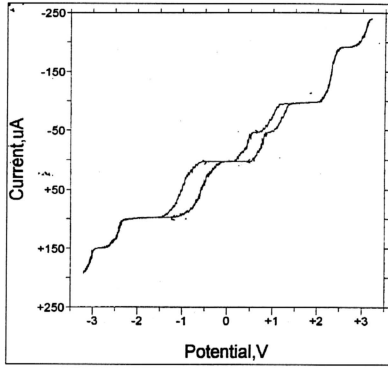

Figure 4.23 : Voltammogram of S3 heated at 800°C.

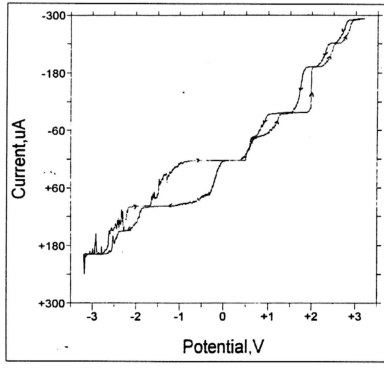

Figure 4.24 ; Voltammogram of S4 heated at 400°C.

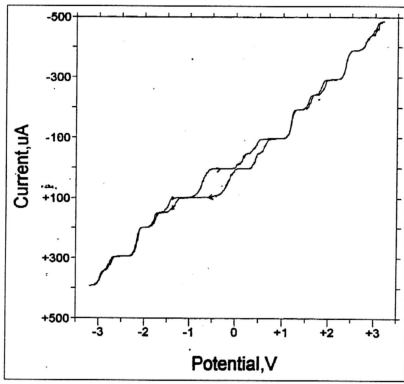

Figure 4.25 : Voltammogram of S4 heated at 800°C.

Cyclic voltammetry for all samples were also done at $400mVs^{-1}$, and there were no double increment in the current. This means that the relationship between current, I and voltage, V as $I \alpha V^{1/2}$ was not observed for all the voltammograms. Therefore the redox couple $Li^+ + e^- \Leftrightarrow Li$ within the matrix is clearly not a diffusion controlled reaction. As for the staircase waves, this can be attributed to the redox couples of the transition metals in the compound, such as $Ni^{III} + e^- \Leftrightarrow Ni^{II}$, $Ni^{II} + e^- \Leftrightarrow Ni^{I}$, $Co^{III} + e^- \Leftrightarrow Co^{II}$ etc. Since the transition metal redox reactions does not involve diffusion, then there are no loops observed. The exact redox potentials for $Li^+ + e^- \Leftrightarrow Li$ in different transition metal intercalations cannot be determined from these set of voltammogram, as more work need to be done on different compounds such as $LiNiO_2$, $LiCoO_2$, etc.

4.6 Battery performance

The battery was assembled in the following configuration:

$$LiNi_{0.7}M_xM'_yM''_{0.3-(x+y)}O_2/electrolyte/C$$

In this configuration, the cell is in the dead mode. So, the cell has to be charged which means that Li^+ in $LiNi_{0.7}M_xM'_yM''_{0.3-(x+y)}O_2$ must de-intercalate enter the electrolyte and intercalate in the anode. When given a current of 50mA for 2 minutes the cell was charged to 2V. When discharge, the Li^+ de-intercalate in the carbon anode and intercalate into cathode active material at the end of its journey. Figure 4.26 shows 3 cycles of charge-discharge curve for the battery using $LiNi_{0.7}Co_{0.3}O_2$ as the cathode active material. The poor performance of the battery can be attributed to a large number of factors such as polarization, poor assembling, very high interfacial resistance and high humidity content. However details study are beyond the scope of this dissertation.

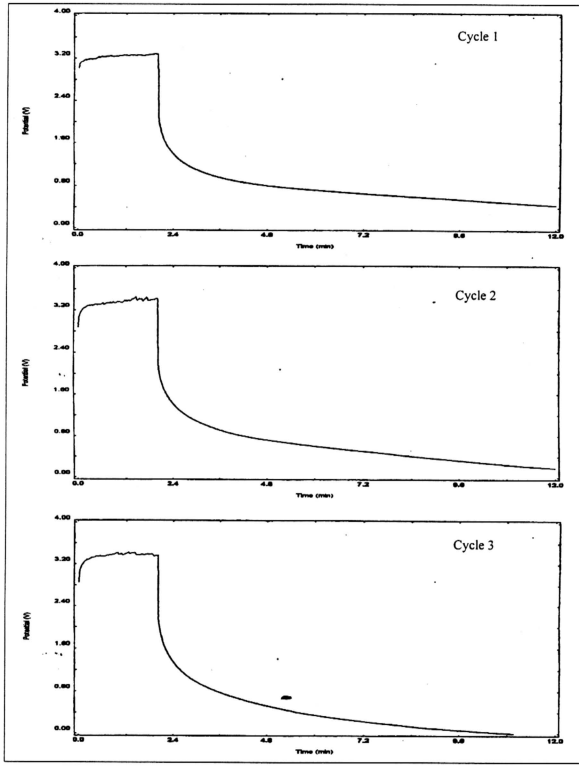

Figure 4.26 : Charge/discharge curves for the battery using $LiNi_{0.7}Co_{0.3}O_2$ as the cathode active material.